

Dynamic optical sampling by cavity tuning and its application in lidar

Lin Yang,¹ Jinsong Nie,^{1,2} and Lingze Duan^{1,*}

¹Department of Physics, University of Alabama in Huntsville, Huntsville, Alabama 35899 USA

²State Key Laboratory of Pulsed Power Laser Technology, Hefei, Anhui 230037 China

*lingze.duan@uah.edu

Abstract: Optical sampling by cavity tuning (OSCAT) enables cost-effective realization of fast tunable optical delay using a single femtosecond laser. We report here a dynamic model of OSCAT, taking into account the continuous modulation of laser repetition rates. This allows us to evaluate the delay scan depth under high interferometer imbalance and high scan rates, which cannot be described by the previous static model. We also report the demonstration of remote motion tracking based on fast OSCAT. Target vibration as small as 15 μm peak to peak and as fast as 50 Hz along line-of-sight has been successfully detected at an equivalent free-space distance of more than 2 km.

©2013 Optical Society of America

OCIS codes: (120.3930) Metrological instrumentation; (320.7090) Ultrafast lasers; (060.4080) Modulation; (070.4550) Correlators; (280.3640) Lidar; (300.6500) Spectroscopy, time-resolved.

References and links

1. J. A. Valdmanis and G. Mourou, "Subpicosecond electrooptic sampling: principles and applications," *IEEE J. Quantum Electron.* **22**(1), 69–78 (1986).
2. W. C. Swann and N. R. Newbury, "Frequency-resolved coherent lidar using a femtosecond fiber laser," *Opt. Lett.* **31**(6), 826–828 (2006).
3. M. R. Hee, J. A. Izatt, J. M. Jacobson, J. G. Fujimoto, and E. A. Swanson, "Femtosecond transillumination optical coherence tomography," *Opt. Lett.* **18**(12), 950–952 (1993).
4. A. Schliesser, M. Brehm, F. Keilmann, and D. W. van der Weide, "Frequency-comb infrared spectrometer for rapid, remote chemical sensing," *Opt. Express* **13**(22), 9029–9038 (2005).
5. N. C. J. van der Valk, W. A. M. van der Marel, and P. C. M. Planken, "Terahertz polarization imaging," *Opt. Lett.* **30**(20), 2802–2804 (2005).
6. A. H. Zewail, "Femtochemistry: atomi-scale dynamics of the chemical bond," *J. Phys. Chem. A* **104**(24), 5660–5694 (2000).
7. V. Sundström, "Femtobiology," *Annu. Rev. Phys. Chem.* **59**(1), 53–77 (2008).
8. J. Szydlo, N. Delachenal, R. Gianotti, R. Walti, H. Bleuler, and R. P. Salathe, "Air-turbine driven optical low-coherence reflectometry at 28.6-kHz scan repetition rate," *Opt. Commun.* **154**(1-3), 1–4 (1998).
9. A. L. Oldenburg, J. J. Reynolds, D. L. Marks, and S. A. Boppart, "Fast-Fourier-domain delay line for in vivo optical coherence tomography with a polygonal scanner," *Appl. Opt.* **42**(22), 4606–4611 (2003).
10. P. A. Elzinga, F. E. Lytle, Y. Jian, G. B. King, and N. M. Laurendeau, "Pump/probe spectroscopy by asynchronous optical sampling," *Appl. Spectrosc.* **41**(1), 2–4 (1987).
11. C. Janke, M. Först, M. Nagel, H. Kurz, and A. Bartels, "Asynchronous optical sampling for high-speed characterization of integrated resonant terahertz sensors," *Opt. Lett.* **30**(11), 1405–1407 (2005).
12. A. Bartels, R. Cerna, C. Kistner, A. Thoma, F. Hudert, C. Janke, and T. Dekorsy, "Ultrafast time-domain spectroscopy based on high-speed asynchronous optical sampling," *Rev. Sci. Instrum.* **78**(3), 035107 (2007).
13. T. Hochrein, R. Wilk, M. Mei, R. Holzwarth, N. Krumbholz, and M. Koch, "Optical sampling by laser cavity tuning," *Opt. Express* **18**(2), 1613–1617 (2010).
14. R. Wilk, T. Hochrein, M. Koch, M. Mei, and R. Holzwarth, "OSCAT: Novel technique for time-resolved experiments without moveable optical delay lines," *J. Infrared Milli. Terahz. Waves* **32**(5), 596–602 (2011).
15. R. Wilk, T. Hochrein, M. Koch, M. Mei, and R. Holzwarth, "Terahertz spectrometer operation by laser repetition frequency tuning," *J. Opt. Soc. Am. B* **28**(4), 592–595 (2011).
16. C. Mohr, A. Romann, A. Ruehl, I. Hartl, and M. E. Fermann, "Fourier transform spectrometry using a single cavity length modulated mode-locked fiber laser," in *Fiber Laser Applications*, OSA Technical Digest (CD), paper FWA2.
17. T. C. Briles, D. C. Yost, A. Cingöz, J. Ye, and T. R. Schibli, "Simple piezoelectric-actuated mirror with 180 kHz servo bandwidth," *Opt. Express* **18**(10), 9739–9746 (2010).

18. P. Balling, P. Křen, P. Mašika, and S. A. van den Berg, "Femtosecond frequency comb based distance measurement in air," *Opt. Express* **17**(11), 9300–9313 (2009).
 19. M. Cui, M. G. Zeitouny, N. Bhattacharya, S. A. van den Berg, H. P. Urbach, and J. J. M. Braat, "High-accuracy long-distance measurements in air with a frequency comb laser," *Opt. Lett.* **34**(13), 1982–1984 (2009).
 20. I. Coddington, W. C. Swann, L. Nenadovic, and N. R. Newbury, "Rapid and precise absolute distance measurements at long range," *Nat. Photonics* **3**(6), 351–356 (2009).
 21. J. Lee, Y. J. Kim, K. Lee, S. Lee, and S. W. Kim, "Time-of-flight measurement with femtosecond light pulses," *Nat. Photonics* **4**(10), 716–720 (2010).
 22. H. Byun, M. Y. Sander, A. Motamedi, H. Shen, G. S. Petrich, L. A. Kolodziejski, E. P. Ippen, and F. X. Kärtner, "Compact, stable 1 GHz femtosecond Er-doped fiber lasers," *Appl. Opt.* **49**(29), 5577–5582 (2010).
-

1. Introduction

Tunable optical delay (TOD) has long been an important technique for spectroscopy and precision optical metrology. The advent of mode-locked femtosecond lasers in the 1990s opened up a new class of applications for TOD: optical sampling [1]. By splitting a femtosecond pulse train into two parts and subsequently recombining them on the sample with a variable time delay, one can make time-resolved measurements in a variety of schemes, such as light detection and ranging (lidar) [2], optical coherence tomography [3], Fourier transform spectroscopy [4], terahertz (THz) time-domain spectroscopy [5], femtochemistry [6], and femtobiology [7].

Two desirable features for TOD are high scan rates and large scan depths. High scan rates lead to high data-updating rates, which are necessary for real-time, dynamic measurements. Large scan depths, meanwhile, are critical for the applications involving long time scales (e.g., > 100 ps). Traditional TOD schemes are based on mechanical systems such as translation stages or rotating mirrors. Their scan rates can reach the kHz range with fast spinning devices [8]. However, at such high scan rates, the scan depths are limited to only 2–3 mm [8,9]. Asynchronous optical sampling (ASOPS) overcomes this limitation by replacing the mechanical delay line with a second femtosecond laser slightly detuned in the pulse repetition rate [10–12]. Since there is no moving component in the system, scans as fast as 100 kHz can be achieved [11], and a time-delay window of 1 ns (equivalent to a 30-cm total scan range) has been demonstrated at a 10-kHz scan rate [12]. However, ASOPS requires an additional femtosecond laser and a complex phase lock system, which add significant cost and complexity to the scheme.

Over the last two years, a novel TOD scheme called optical sampling by cavity tuning (OSCAT) has been proposed and demonstrated [13–16]. OSCAT combines a highly imbalanced interferometer with intracavity tuning of the pulse repetition rate to create a scan of the relative pulse delay. Its basic principle is illustrated in Fig. 1. As a pulse train propagates through an imbalanced interferometer, pulses meeting at the output port via different arms originate from different parts of the input pulse train. If the pulse spacing in the input pulse train is temporally modulated, the interferometer translates the modulation into a scan of relative pulse delay at its output port. The modulation can be realized through a dither of the laser cavity length. Since most femtosecond lasers today (solid-state or fiber lasers) tune their cavity lengths using piezo-electric (PZT) actuators, whose operating bandwidth can be greater than 100 kHz [17], the scan rate of OSCAT can potentially reach 100 kHz or even higher. This is ideal for achieving fast update rates in time-resolved measurements such as pump-probe spectroscopy, *in situ* bio-imaging, and lidar.

Compared with other TOD techniques, OSCAT excels in both performance and cost. Although OSCAT still involves mechanical movement, the fact that the tuning occurs inside the laser cavity allows a small length variation to produce a large time delay. This magnification of scale (see detailed analysis in Section 2) leads to improvement in both scan rate and scan depth from conventional mechanical TOD. On the other hand, OSCAT is capable of reaching comparable performance as ASOPS without the need for a second femtosecond laser and the phase-lock electronics, which is a significant improvement in cost-effectiveness and compactness.

So far, OSCAT has been demonstrated in terahertz spectrometry [15] and Fourier-transform spectrometry [16]. A simple theory based on fixed pulse repetition rates has also been formulated to describe the dependence of the relative pulse delay on repetition rate variations [13,14]. This static model, however, does not take into account implementations where the laser repetition rate is continuously modulated. It is only valid when the modulation cycle is much longer than the time delay caused by the interferometer imbalance. For applications involving fast modulation frequencies (e.g., > 1 kHz) or large interferometer imbalance (e.g., > 1 km), a dynamic model considering the temporal variation of the laser repetition rate must be used. In the present paper, we first describe the formulation of such a theoretical model. We then report an experimental demonstration of OSCAT-based remote motion tracking using a Mach-Zehnder interferometer (MZI) with a km-scale imbalance. Similar time-of-flight distance measurement based on optical sampling has been reported by several groups recently using mechanical delay lines [18,19], ASOPS [20] and phase-locking control of the repetition rate [21]. Our study here focuses on the potential of OSCAT in tracking the dynamic movements of a target, and our scheme does not require phase locking. The technique may prove to be a cost-effective solution for future femtosecond lidars.

2. A dynamic model of OSCAT

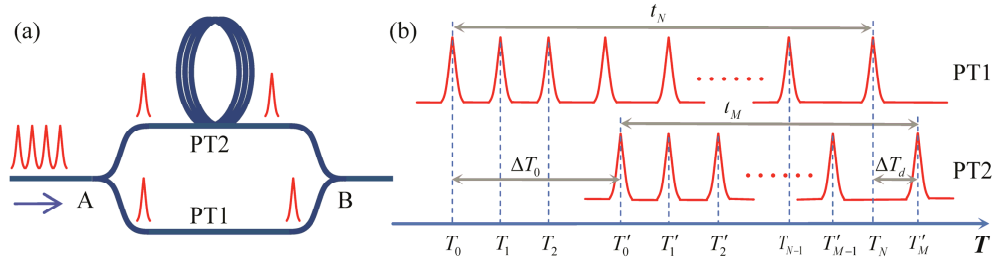


Fig. 1. The basic principle of OSCAT: (a) an imbalanced Mach-Zehnder interferometer creates relative pulse delay at the output port, and (b) a modulation of the pulse repetition rate results in a scan of the pulse delay at the modulation frequency.

We begin by considering a conceptually simple Mach-Zehnder interferometer (MZI), as shown in Fig. 1(a), with one arm much longer than the other. A pulse train with a modulated repetition rate enters the interferometer at Port A and is split evenly into two parts. The two pulse trains, denoted here as PT1 and PT2, gain a relative delay after traveling through the two arms of the MZI and meet again at Port B. If the arrival time of each pulse from both pulse trains is recorded at Port B, we will obtain two series of temporal marks, labeled as T_N and T'_M in Fig. 1(b), with N and M being the indices of the pulses in the original pulse train. In other words, T_N and T'_N represent the arrival times of the same pulse via the short and the long arms of the MZI, respectively. With this definition, it is immediately clear that $T'_N - T_N = \Delta T_0$, where ΔT_0 is the time delay between the two pulse trains caused by the interferometer imbalance. What we need to find out here is the relative delay between the N th pulse in PT1 and its closest follower from PT2, say the M th pulse (see Fig. 1(b)). Here we use ΔT_d to represent this delay. Note that, while ΔT_0 is a constant depending only on the imbalance, ΔT_d is a time-dependent variable owing to the repetition rate modulation. It is ΔT_d that leads to the scan of the pulse delay.

For a general discussion, we first assume the pulse repetition rate is an arbitrary periodic function of time, $S(t)$, with a modulation frequency f_m . We further assume $S(0)$ coincides with a reference pulse, which is given an index 0. For PT1, the time of the N th pulse arriving at Port B can be expressed as

$$T_N = T_0 + \sum_{i=1}^N \frac{1}{f_{Ri}}, \quad (1)$$

where T_0 is the arrival time of the reference pulse, and f_{Ri} is the instantaneous repetition rate at the i th pulse. f_{Ri} can be written as

$$f_{Ri} = f_{R0} + \Delta f_R \cdot S(t_i), \quad (2)$$

where f_{R0} is the nominal repetition rate, Δf_R is the amplitude of repetition rate modulation, and $S(t_i)$ is the value of $S(t)$ at the time of the i th pulse (see Fig. 1(b)). Note that we can assume $-1 \leq S(t_i) \leq 1$ without losing any generality. Substituting Eq. (2) into Eq. (1) and assuming $\Delta f_R / f_{R0} \ll 1$ (normally $\Delta f_R \sim \text{kHz}$ and $f_{R0} \sim 100 \text{ MHz}$) yields the following general expression for the arrival time of the N th pulse in PT1,

$$T_N = T_0 + \frac{N}{f_{R0}} - \frac{\Delta f_R}{f_{R0}^2} \sum_{i=1}^N S(t_i). \quad (3)$$

A similar derivation can be made for the M th pulse in PT2,

$$T'_M = T'_0 + \frac{M}{f_{R0}} - \frac{\Delta f_R}{f_{R0}^2} \sum_{i=1}^M S(t_i). \quad (4)$$

Subtracting Eq. (3) from Eq. (4) leads to

$$\Delta T_d = \delta T_0 + \frac{\Delta f_R}{f_{R0}^2} \sum_{i=M+1}^N S(t_i), \quad (5)$$

where $\delta T_0 \equiv \Delta T_0 - (N - M) / f_{R0}$ is a small offset duration resulting from the difference between ΔT_0 and the total duration of $(N - M)$ pulses. It is not difficult to show that δT_0 is less than one pulse interval, i.e., $0 < \delta T_0 < 1 / f_{R0}$. Eq. (5) is a general expression of ΔT_d in a summation form. In practice, it is often more convenient to use an integration form. This can be done by rewriting Eq. (5) as

$$\Delta T_d = \delta T_0 + \frac{\Delta f_R}{f_{R0}^2} \sum_{i=M+1}^N S(t_i) \cdot \Delta t_{R0} \approx \delta T_0 + \frac{\Delta f_R}{f_{R0}^2} \int_{t_M}^{t_N} S(t) dt, \quad (6)$$

where $\Delta t_{R0} \equiv 1 / f_{R0}$ is the nominal pulse interval. Note that, to get Eq. (6), we have assumed $f_m \ll f_{R0}$ and $N - M \gg 1$. The first assumption simply reflects the fact that the modulation frequency ($< 100 \text{ kHz}$) is much less than the pulse repetition rate ($\sim 100 \text{ MHz}$) and the second one requires the MZI imbalance to be much greater than the pulse spacing.

So far, the analysis has been based on a generic modulation function $S(t)$. In practice, sinusoidal modulation is commonly used. Much insight can be gained by exploring this simple yet important case. Substituting $S(t) = \sin 2\pi f_m t$ into Eq. (6) yields

$$\Delta T_d(t_M) = \delta T_0 + \frac{\Delta f_R}{f_{R0}^2} \frac{\sin(\pi f_m \Delta t_{NM})}{\pi f_m} \sin \left[2\pi f_m \left(t_M + \frac{\Delta t_{NM}}{2} \right) \right], \quad (7)$$

where $\Delta t_{NM} \equiv t_N - t_M$. Under the large-imbalance assumption, Δt_{NM} can be replaced by the interferometer imbalance ΔT_0 without losing much accuracy since they are only different by

ΔT_d (see Fig. 1(b)), which is less than one pulse interval. Also, since the pulse repetition rate is normally very fast, we can simply replace t_M with t in Eq. (7) and treat ΔT_d as a continuous function. We then consider the important special case of slow modulation, i.e., $f_m \Delta T_0 \ll 1$, and simplify Eq. (7) to

$$\Delta T_d(t) \approx \delta T_0 + \frac{\Delta f_R \Delta T_0}{f_{R0}} \sin \left[2\pi f_m \left(t + \frac{\Delta T_0}{2} \right) \right]. \quad (8)$$

Equations (7) and (8) give a dynamic description of the temporal variations of the relative pulse delay under a sinusoidal modulation in an OSCAT scheme. Several interesting conclusions can be drawn from the two equations. The modulation of the pulse repetition rate creates a pulse-delay scan at the same frequency with an additional phase lag roughly equal to $\pi f_m \Delta T_0$. The center value of this scan can be adjusted by an offset delay δT_0 , which offers an extra degree of freedom if certain absolute values of ΔT_d is needed. The delay scan depth is proportional to the product of the relative modulation amplitude, $\Delta f_R / f_{R0}$, and the interferometer imbalance, ΔT_0 . Since $|\Delta f_R / f_{R0}| = |\Delta L_c / L_{c0}|$, where ΔL_c and L_{c0} are the cavity length variation and the nominal cavity length, respectively, OSCAT can be viewed as equivalent to a delay line with a tuning range

$$\Delta L_d = (\Delta L_i / L_{c0}) \Delta L_c, \quad (9)$$

where ΔL_i is the interferometer imbalance in terms of length. High-repetition-rate femtosecond lasers usually have a cavity length $L_{c0} \sim 0.1-1$ m. If the interferometer imbalance is $\Delta L_i = 1$ km, the ratio between the equivalent delay-line tuning range and the actual variation of cavity length are related by $\Delta L_d / \Delta L_c = \Delta L_i / L_{c0} \sim 10^3 - 10^4$. This clearly demonstrates that, by using intracavity modulation and a large interferometer imbalance, one can substantially magnify the effect of a small cavity length variation to create a large TOD.

However, the scaling factor $\Delta L_i / L_{c0}$ will not increase indefinitely with the increase of ΔL_i (or equivalently ΔT_0). When the imbalance becomes so large that the condition $f_m \Delta T_0 \ll 1$ is no longer satisfied, one has to describe the relative pulse delay with Eq. (7), which shows that the scan depth peaks when $\Delta T_0 = 1/2f_m$ and vanishes when $\Delta T_0 = 1/f_m$. The dependence of the scan depth on the modulation frequency and the imbalance of the interferometer is summarized in Fig. 2(a), where $\Delta f_R = 3.55$ kHz and $f_{R0} = 250$ MHz have been assumed. The “ridge” diagonally across the center corresponds to the parameter region where peak scan depths can be reached. Moreover, Fig. 2(a) indicates that the scan depth achievable with a certain imbalance also depends on the modulation frequency (or scan rate). Figure 2(b) shows how scan depth, expressed as the equivalent delay line length, is related to the imbalance at three different modulation frequencies: 1 kHz, 10 kHz and 20 kHz. According to Fig. 2(b), which can be viewed as the cross sections of Fig. 2(a) at these three frequencies, the scan depth is independent of frequency when the condition $f_m \Delta T_0 \ll 1$ is satisfied, which is the regime described by Eq. (8). As ΔT_0 increases, faster scans begin to crest while slower scans continue to grow in depth. Thus, in practice, there is a tradeoff between the scan rate and the scan depth when the interferometer imbalance is sufficiently large.

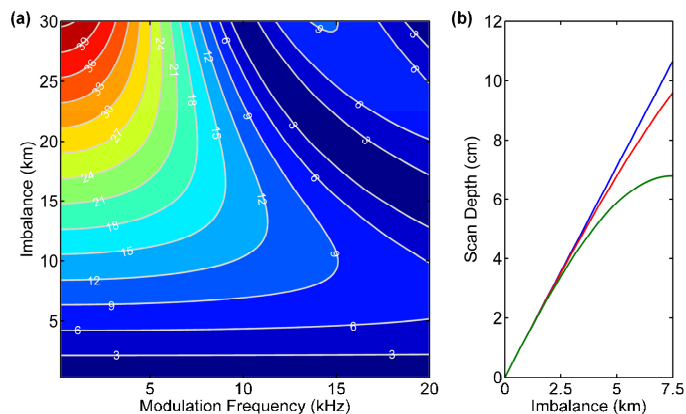


Fig. 2. The scan depth of OSCAT: (a) the dependence of the scan depth (in the unit of cm) on the modulation frequency and the interferometer arm-length imbalance, and (b) scan depth vs. imbalance for three special cases of the modulation frequency: 1 kHz (blue), 10 kHz (red), and 20 kHz (green).

Finally, attention should be given to the scale of the scan depth. With realistic values of Δf_R and f_{R0} , an imbalance of a few kilometers, and a scan rate of 1–20 kHz, a scan depth of several centimeters (or $\Delta T_d \sim 100$ ps) can be produced. Such performance is adequate for most time-resolved measurements.

3. Remote motion tracking with OSCAT

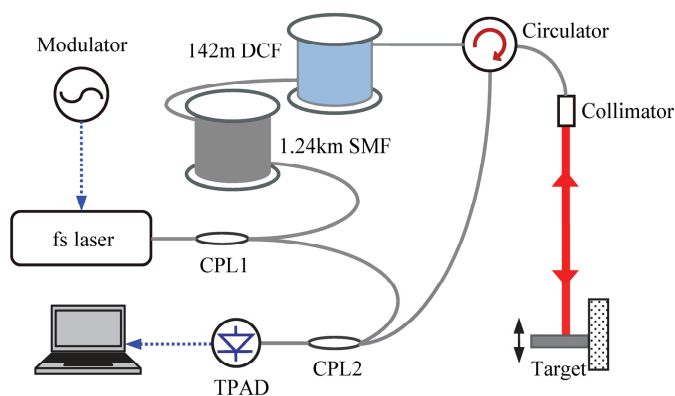


Fig. 3. Schematic of the experimental system for OSCAT target motion tracking. CPL, optical coupler; DCF, dispersion compensating fiber; SMF, single-mode fiber; and TPAD, two-photon absorption detector.

As pointed out in the previous section, a key element in the OSCAT scheme is a long arm-length imbalance (\sim km) in the interferometer. Whereas this requirement may pose technical difficulties for certain lab-based measurements, it naturally fits those applications involving long pulse-propagation distances, such as lidar and remote sensing. In lidar, for example, one can simply use the optical path to be measured as the long arm of the interferometer. By pairing it with a short arm, whose length is precisely known, and measuring the relative pulse delay ΔT_d , one can deduce the interferometer imbalance and, hence, the total length of the long arm. Furthermore, since ΔT_d can be updated as fast as 100 kHz, the line-of-sight motion of the target can be tracked in real time, which allows the target velocity, or even the

acceleration, to be derived. This makes the technique a suitable option for real-time target motion tracking.

In the present work, we aim to experimentally demonstrate the capability of an OSCAT system in tracking fast movement of a distant target along the line-of-sight direction. A schematic of the experimental setup is shown in Fig. 3. The light source is a femtosecond fiber laser (MenloSystems M-Comb) operating near 1560 nm with a pulse repetition rate of 250 MHz. The laser is equipped with an internal translation stage, which allows the repetition rate to be changed by up to 2.5 MHz. In addition, a high-speed PZT actuator (20 kHz bandwidth) allows fast tuning of the repetition rate by as much as 3.55 kHz. The laser output is split at a fiber coupler (CPL1) and coupled into a highly imbalanced MZI. The short arm is a 5.34-m fiber link, whereas the long arm consists of the optical path to the target. In order to simulate a distant target in this table-top, proof-of-principle experiment, we insert a 1.38-km fiber link into the long arm. The optical power coupled into the fiber link is about 32 mW. A collimator at the end of the fiber link couples the light into a 0.55-m free-space link where a mirror mounted on a translation stage serves as the target. The pulses reflected by the target are collected by the collimator and routed by a circulator to the output fiber coupler (CPL2), where they are combined with the pulses from the short arm. A two-photon absorption detector (TPAD) is used to measure the cross-correlation between the pulses from the two arms. The detector is made of a 910-nm light-emitting diode with its cap removed. The correlation traces are acquired by an oscilloscope, and the data are analyzed by a computer.

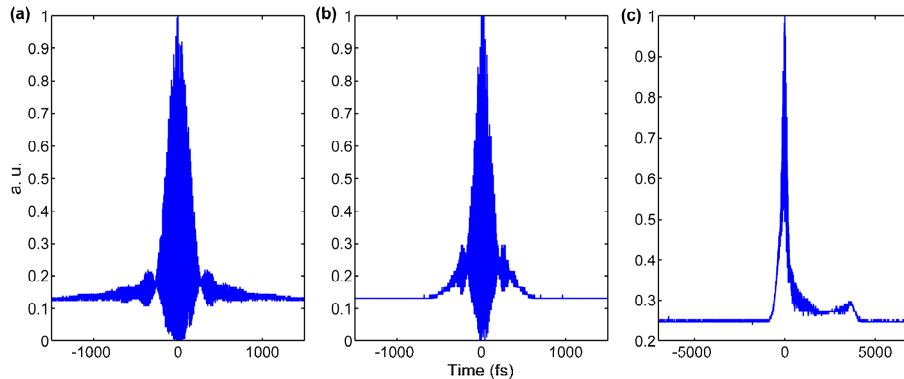


Fig. 4. (a) The autocorrelation trace of the delayed pulse after it propagates through the long arm, a 1.38-km dispersion-compensated fiber link, (b) the autocorrelation trace of reference pulse from the short arm, and (c) the second-order cross-correlation trace of the two pulses.

A crucial component for the experiment is the long fiber delay line. Since the pulses directly from the laser are about 150 fs long, careful dispersion compensation is necessary in order to counter balance the severe pulse broadening incurred by the long fiber. To that end, we splice a 142-m section of dispersion compensating fiber (DCF) after a 1.24-km section of single-mode fiber (SMF-28). The length of the single-mode fiber is cut in such a way that the autocorrelation measured at the TPAD is minimized for the delayed pulses coming from the long arm. A typical such autocorrelation trace is shown in Fig. 4(a). The main peak of the pulse is estimated to have a full width at half maximum (FWHM) of roughly 500 fs. Similar dispersion compensation is also done for the reference pulses by inserting a short section of DCF into the short arm. Pulses about 400 fs wide have been obtained as shown by the autocorrelation trace in Fig. 4(b). Once the pulses from both arms are optimized separately, their cross-correlation is measured, with a typical trace shown in Fig. 4(c). The FWHM of the cross-correlation trace is about 700 fs. The asymmetric shape is mainly due to uncompensated higher-order dispersion (especially in the long arm), which leads to asymmetric pulse shapes.

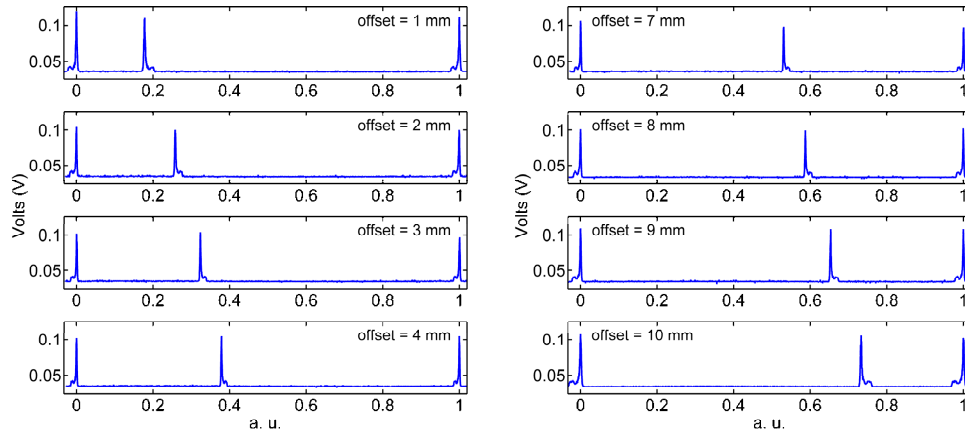


Fig. 5. Cross-correlation traces with various target displacements from the reference point. There is a clear correlation between the cross-correlation peak separation and the target displacement. The horizontal scale is normalized to the maximum range achievable with the PZT scan. A scan depth of more than 10 mm (or a maximum round-trip delay of more than 20 mm) has been experimentally realized.

With the cross-correlation measured, we are ready to determine the displacement of the target from its nominal position using OSCAT. Our approach is similar to that used in Ref [19]. However, the cross-correlation traces are produced by scanning the laser repetition rate instead of the reference-arm length. Specifically, we first tune the repetition rate so that the pulses from both arms overlap on the TPAD. This is done by sweeping the internal stage of the laser across a relatively large range. Once this reference point is found, we then fix the internal stage and begin to modulate the PZT actuator. Each cycle of the PZT scan produces two cross-correlation traces, one for each trip. The two traces would overlap if the position of the target and the pulse repetition rate are matched in such a way that pulse overlapping occurs at either end of the PZT movement. Any displacement from this reference position would cause the two cross-correlation traces to separate, and their temporal separation is a direct function of the target displacement from the reference point. Figure 5 shows a series of cross-correlation measurements with the target gradually tuned away from the reference point at a 1-mm increment. When we align one of the cross-correlation traces from all the measurements and set them at zero, the location of the other cross-correlation trace clearly depends on the target offset. The third cross-correlation trace on the far right is caused by the next PZT scan cycle. It also corresponds to the maximum displacement range that can be measured by OSCAT. With our current setup, a total round-trip delay of more than 20 mm has clearly been achieved.

In order to make actual displacement measurement, a calibration curve between the cross-correlation spacing (in terms of time) and the target displacement needs to be determined. This can be done either through a series of simultaneous measurements of both quantities or via theoretical prediction given by Eq. (7) or Eq. (8) with predetermined knowledge of Δf_R (through the PZT specifications) and ΔT_0 . Fig. 6(a) shows such calibration curves from both approaches at a modulation frequency $f_m = 1$ Hz. The experimental data and the theoretical prediction agree fairly well except for a slight deviation near the middle of the curve. Likely causes of the discrepancy are slight nonlinear response of the PZT actuator and small drift of the repetition rate during the course of the calibration. Note that the calibration curve is dependent on the modulation frequency. For each PZT scan frequency, a unique calibration curve needs to be measured.

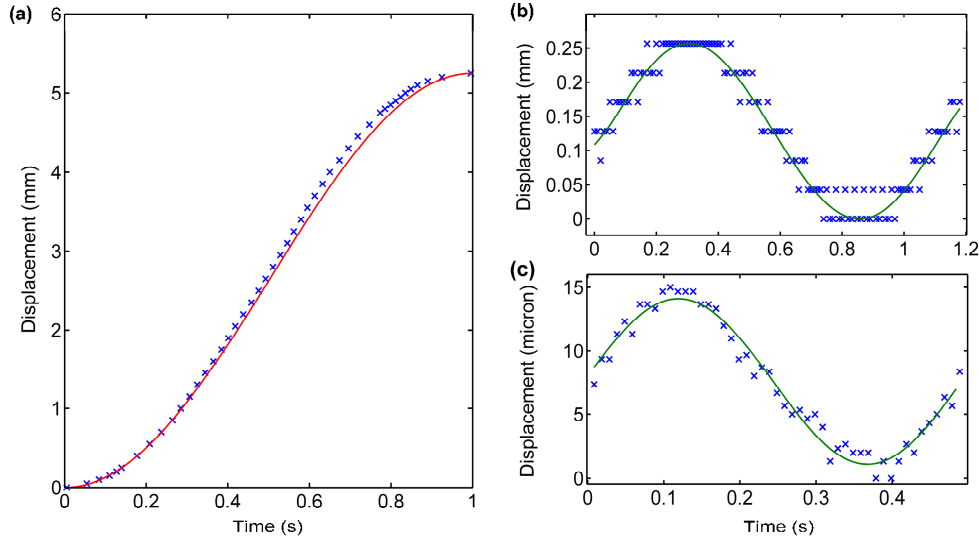


Fig. 6. OSCAT displacement measurement: (a) a sample calibration curve based on experiment (check markers) and theoretical prediction (solid line); (b) OSCAT-measured displacements (check markers) and trajectory prediction (solid line) when the target oscillates at 1 Hz along the line-of-sight direction; and (c) a similar tracking result with the target oscillating at about 2 Hz with a peak-to-peak amplitude of only 15 μm . The 40- μm displacement resolution in (b) is caused by the slow (10 kHz) data sampling rate. Such a limitation is eliminated in (c) by raising the sampling rate to 260 kHz.

To demonstrate dynamic motion tracking, we let the target oscillate along the line-of-sight direction by driving the translation stage with a step motor. We then modulate the PZT at a much higher frequency and use an oscilloscope (or a voltmeter) to take a series of consecutive cross-correlation measurements. The recorded data are sent to a computer, where they are converted into a series of displacement values (with the help of a calibration curve for the pertinent frequency). Since the displacement measurement relies on the measurement of cross-correlations and precise measurement of pulse cross-correlations requires fast sampling, a data-acquisition system capable of high-speed sampling and buffering is indispensable for dynamic OSCAT motion tracking. Figure 6(b) shows the measured target displacements over a full oscillation cycle (blue marks), along with the recovered target trajectory (green curve), when the target oscillates at 1 Hz and the PZT scans at 100 Hz. The oscilloscope used for this measurement can only take a total of 10,000 sampling points. Therefore, in order to measure a full oscillation cycle, the sampling rate has to be set at 10 kHz, i.e. 100 points per PZT cycle. Such a slow sampling is not sufficient to resolve the details of the cross-correlation trace, leading to the step-like trace with an increment of about 40 μm . By increasing the sampling rate and hence the total number of sampling points, the displacement resolution can be much improved. Figure 6(c) shows a similar measurement with a target oscillation frequency of 2 Hz, a PZT scan rate of 100 Hz, and a data sampling rate of 260 kHz. A target oscillation 15- μm peak-to-peak is recovered with high resolution.

To demonstrate the tracking of much faster movement, we replace the target with a mirror attached on a speaker. We then drive the speaker with a sinusoidal signal to generate a line-of-sight vibration at chosen frequencies. A second mechanism to track the mirror displacement is introduced to calibrate the actual motion of the mirror. This is done by slightly misalign the incident beam so that the longitudinal vibration introduces a variation of the received optical power. Figure 7(a) shows OSCAT-measured speaker vibration when the speaker is driven at 50 Hz and the PZT scans at 500 Hz. Note that the OSCAT scan is calibrated in this case so the measurement is able to specify the actual vibration amplitude of the speaker. To make sure what we see through OSCAT is indeed what happens on the

speaker, we overlay the OSCAT trace with traces from the optical power measurement and the driving signal to the speaker. The result, as shown in Fig. 7(b), further confirms a faithful recovery of the speaker motion by OSCAT.

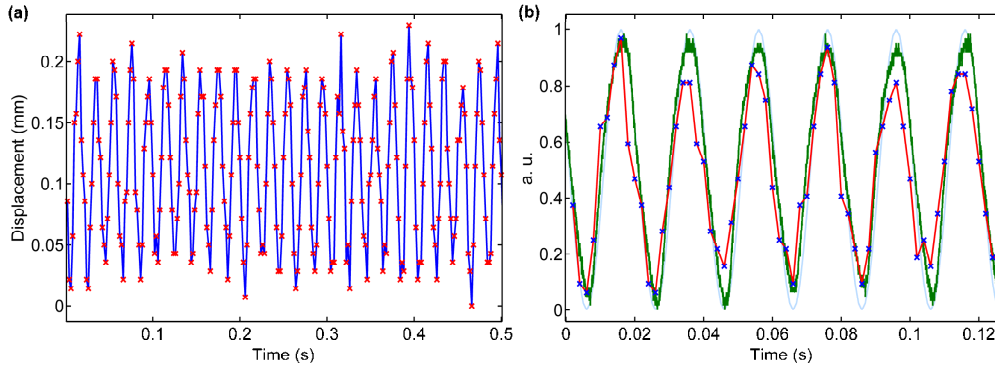


Fig. 7. OSCAT lidar tracks fast target movement: (a) OSCAT detected speaker vibration at 50 Hz; (b) a close look of a part of trace (a) (check marker, red trace) along with the trace from the auxiliary tracking method (green) and the modulation signal to the speaker (light blue).

4. Discussion and conclusion

It should be stressed here that the results shown above are only for proof of principles. Several engineering upgrades can be made to enhance the applicability of the OSCAT scheme. In the demonstration above, target trajectories are recovered through post-measurement analysis. For real-time motion tracking, an integrated data buffering and processing system is needed. Also, for tracking high-speed target movement, higher PZT scan rates are necessary. For our laser, stable cross-correlation traces have been measured at rates as high as 1 kHz. Faster scans were not tested in the present work out of concerns of the long-term mechanical stability of the PZT-mirror assembly, but no fundamental restrictions prevent this from being carried out. In fact, the PZT actuator in our laser has a bandwidth of 20 kHz, and PZT actuated intracavity mirrors with bandwidths close to 200 kHz have been demonstrated [17]. Besides mechanical stability, pulsing dynamics could be a limiting factor for the scan rate as rapid modulations of the cavity length may disturb the establishment of stable pulsing. In our experiment, pulse broadening is observed at the 1-kHz scan rate, indicating the change of intracavity dynamics. However, from an application point of view, as long as the laser can supply a stable cross-correlation, the OSCAT scheme is feasible. By using lasers with higher repetition rates, such as a highly-stable GHz femtosecond fiber laser [22], the potential limitation set by pulsing stability can be further relaxed.

Scan depth is another important parameter for displacement measurement. It determines the range of displacement that can be tracked by the PZT modulation. We have demonstrated an OSCAT scan depth of more than 10 mm as shown in Fig. 5. This range can potentially be increased to tens of centimeters (see Fig. 2(a)) with longer interferometer imbalances (i.e., larger ΔT_0 in Eq. (8)), longer PZT actuators (higher Δf_R), stronger modulation (higher Δf_R), and shorter laser cavities (greater ratio of $\Delta f_R / f_{R0}$). When the target movement is beyond this range, a separate intracavity mechanism with larger tuning depth is needed to shift the reference point. In our experiment, this is done by moving the intracavity translation stage, which has a much slower response but a much greater tuning range ($\Delta f_R \sim 2.5$ MHz) compared to the PZT actuator.

So far, our discussion has focused on the measurement of displacement. In practice, it is often equally important to determine the absolute distance of the target. In our experiment, the nominal distance of the target, i.e., the absolute distance of the reference point, is measured by tuning the intracavity translation stage so that two consecutive pulse overlaps are detected.

The corresponding pulse repetition rates, f_{o1} and f_{o2} , are related to the interferometer imbalance ΔT_0 through the simple relation $\Delta T_0 = 1/(f_{o2} - f_{o1})$. Since the length of the short arm is precisely known, the length of the long arm can be derived. We have measured the difference between f_{o1} and f_{o2} to be 148.64 kHz. This is translated to a 2.02-km free-space distance or, in our case, 1376 m in fiber and 0.546 m in free space, from the laser.

In conclusion, we have presented here an in-depth study of OSCAT. Theoretically, a dynamic model of OSCAT has been formulated to describe the temporal dependence of the relative pulse delay on the pulse repetition rate modulation. It shows that a long interferometer imbalance (e.g., > km) can substantially magnify the effect of a small intracavity tuning to produce a large delay scan. The model also reveals a close relation between the scan rate and the scan depth when a highly imbalanced interferometer is used. Such a relation is absent in the previous static model. Experimentally, we have demonstrated remote tracking of target motions based on dynamic OSCAT. Target vibration has been successfully detected at an equivalent free-space distance of more than 2 km, with line-of-sight oscillations as small as 15 μm peak-to-peak and as fast as 50 Hz faithfully detected. Scan rates up to 1 kHz have been experimentally demonstrated with our current OSCAT system. However, much higher scan rates are in principle feasible with wide-bandwidth PZT actuators and GHz femtosecond lasers. The technique offers a ready solution for lidar as the large interferometer imbalance is naturally supplied by the long target distance and the rapid delay scan enables fast motion tracking.

Acknowledgment

This work was jointly supported by the National Science Foundation under Grant ECCS-1040019 and NASA EPSCoR under Grant NNX07AL52A.